

# Materials and Device Design for Epidermal UV Sensors with Real-Time, Skin-Color Specific, and Naked-Eye Quasi-Quantitative Monitoring Capabilities

Zihang Yang, Jingyang Zhao, Chao Liang,\* and Hanqing Jiang\*

Ultraviolet radiations (UVR) sensors provide quantitative and continuous measurement of UV-induced dermal damage. The challenge though is to develop a sensor that simultaneously offers high sensitivity and rapid response to UVR, as well as compatibility to human skin and skin color specificity. In this paper, an epidermal UV sensor that uses new sets of material and device design strategies to deliver accurate UV intensity measurements is presented. The developed sensor provides real-time and reversible detection performance (color change and recovery) in less than 30 s. By combining the UV photochromic and absorptive materials, a variety of personalized UV epidermal stickers can be developed to achieve naked-eye quasi-quantitative monitoring of UV exposure while simultaneously meeting the specific needs of different skin types. Experimental demonstrations validate the high applicability of these wearable UV sensors for managing the impact of UVR in the daily life.

## 1. Introduction

Ultraviolet radiation (UVR) can be a double-edged sword. It is harmful for human beings and can cause skin aging, wrinkling, burning<sup>[1]</sup> including more deadly skin diseases such as melanoma.<sup>[2]</sup> Australia, for example, has the highest skin cancer rate in the world,<sup>[3]</sup> with 1,170 per 100 000 people diagnosed with melanoma,<sup>[4]</sup> and treatment costs estimated at more than \$700 million annually.<sup>[5]</sup> Conversely, use of UVR is extensively prevalent in industry, medical research, and life, in general. A modest dose of UVR in the form of sunlight exposure is

essential for the body to produce Vitamin D.<sup>[6]</sup> Similarly, UVR is seen as one of the simplest and most effective methods to kill bacteria, virus, yeast, and fungi.<sup>[7–9]</sup> In fact, during the recent pandemic, UVR was reported to have valuable disinfectant properties against Covid-19,<sup>[10]</sup> inactivating and killing 99.9% SARS-CoV-2 virus with UVR (280 nm) of 375 W m<sup>-2</sup>. Balancing UVR intensity is, therefore, is key to maintaining its functionality in the human body, which is why an efficient monitoring sensor is desirable for making safe and effective UVR exposure measurements.


At present, UV sensor technologies can be classified into two major categories. Photoelectric sensors use semiconductor materials for transforming UV illumination into electrical output, wherein metal oxide-based semiconductors such as

ZnO,<sup>[11]</sup> TiO<sub>2</sub>,<sup>[12]</sup> and NiO<sup>[13]</sup> as well as metal nitrides,<sup>[14]</sup> metal sulfides,<sup>[15]</sup> and carbon-based materials<sup>[16]</sup> tune their bandgap in the UV region of the spectrum. Photoelectric UV sensors generally offer high sensitivity and can detect low UV intensity; however, they typically require bulky equipment to generate external electric fields for both operation and measurement of changes during photoexcitation. Photochromic sensors are the second type of UVR sensors. These user-friendly sensors do not require an electrical input and are based on the photochemical reactions that lead to a color change, which can be monitored by the naked eye. Photochromic sensors, however, suffer from low sensitivity and can only provide qualitative rather than quasi-quantitative UVR results. This can be attributed to the fact that the photochromic materials in these sensors change rapidly from one photostate to another with subtle color changes under different intensities of UVR. Therefore, many of these sensors adopt a filter containing UV absorption materials to tune the dose of UVR that makes the photochromic material display the visible color gradient.<sup>[17–19]</sup> However, this design is flawed in that the visible region of the spectrum is also blocked by the filter, making the filter less transparent and further reducing its detection sensitivity. Monitoring results from most photochromic sensors have to be analyzed by auxiliary equipment such as a smartphone,<sup>[20]</sup> which tends to compromise their practical usefulness, as it becomes difficult to monitor UV exposure levels in real-time. Commercially available UVR monitoring products are generally based on the above-mentioned two types of sensing technologies. While the digital UV

Z. Yang, J. Zhao, C. Liang, H. Jiang  
School of Engineering  
Westlake University  
Hangzhou 310030, China  
E-mail: liangchao@westlake.edu.cn; jianghanqing@westlake.edu.cn

Z. Yang  
Vantronics Hangzhou Intelligence Technology Ltd.  
Hangzhou 311100, China

H. Jiang  
Research Center for Industries of the Future  
Westlake University  
Hangzhou, Zhejiang 310030, China

 The ORCID identification number(s) for the author(s) of this article can be found under <https://doi.org/10.1002/admt.202201481>.

DOI: 10.1002/admt.202201481

sensor<sup>[21]</sup> (Shade, Shade, USA) provides accurate UVR results, it needs mechanically hard components (i.e., battery, circuits, and screens), which are expensive and incompatible with direct application to the human skin. The colorimetric sensors<sup>[22]</sup> (My UV patch, L'Oréal, France) involve no hard components and can be applied directly to the human skin, but their degree of accuracy is also limited.

When developing UV sensors for monitoring human exposure to solar radiation, skin-color specificity is another important factor for consideration. As different skin types (types I–VI for lighter to consistently darker color) have different levels of UV tolerance,<sup>[23]</sup> the use of UV sensors needs to be associated with a particular skin type. Compared with the darker skin, the fairer colored skin can only tolerate lower quantities of UV radiation before causing erythema.<sup>[24]</sup> That is to say, the dose of UVR for dark-skinned people to produce vitamin D may exceed the tolerance threshold while causing damage to people with lighter color skin. It is debatable for the current approach of one-fits-all UV sensors, considering the contradictory relationship between the harmful versus beneficial effects of UV radiation. This challenge can be potentially addressed by covering the UV sensor with optical filters, which alter the UV intensity reaching the UV sensor.<sup>[25,26]</sup> However, these filters are usually plastic films, whose rigidity makes it uncomfortable when applied to the human skin. In addition, when dealing with darker skin types, multilayer filters are required, which in turn reduces the transparency of the UV sensor and hinders the naked-eye monitoring performance.

An ideal UV sensor should be of high sensitivity (to provide accurate detection results at low UV intensity), as well as user-friendly (to quantitatively monitor the UV intensity by the naked eye without auxiliary equipment). It must also offer rapid response to sun exposure (to report the UV intensity in real-time), skin-color specificity (to be applicable for people with different skin types), and compatibility to the human skin (to ensure similar skin modulus, comparable detection performance with the human skin, and be easy to apply sunscreen for protection). To the best of our knowledge, UV sensors, to date, that simultaneously possess all these features have yet to be reported.

In this paper, a new method for developing epidermal UV sensors is proposed. Series of photoswitchable pigments are used as the colorimetric chemistry capable of detecting UV power as low as  $0.1 \text{ W m}^{-2}$  and providing real-time detection performance (color change and recovery within 30 s). The 2-(2'-hydroxy-3',5'-di-tert-butylphenyl)-5-chlorobenzotriazole (HD-CB) with different concentration is used as the filter material to block the UV region of the spectrum in a gradient manner without compromising its transparency (transmittance above 80%). Screen printing and lamination are used to integrate the colorimetric and filter materials within the soft material polydimethylsiloxane (PDMS); based on this technique different types of UV sensors can be designed and fabricated to enable important features such as quasi-quantitative naked-eye monitoring, long-term application (working more than 30 cycles without compromising the performance), real-time detection performance, as well as skin-color specificity and compatibility to human skin (Figure 1a). Our UV sensor is practical and convenient for users, which suggest new opportunities for wearable UV detection systems.

## 2. Results and Discussions

### 2.1. Materials and Design of the UV Sensor

The UV sensor is comprised of four layers: a skin-specific layer, UV absorptive layer, UV photochromic layer, and a white background layer (Figure 1b), with each layer of 25  $\mu\text{m}$  in thickness. The skin-specific layer is made from a mixture of absorptive materials and PDMS. By tuning the concentration of absorptive material in the skin-specific layer, the UV intensity reaching the UV sensing area can be adjusted and thus, the customized sensors for people with different skin types can be achieved. The UV absorptive layer is designed to include several UV filtering parts, and each part has a different concentration of absorptive materials. When a low UV intensity is applied, the UV energy goes through the low concentration filtering areas, resulting in a colorimetric change from the photochromic materials underneath. However, the filtering areas with medium and high concentrations can still block UV exposure, and the photochromic materials that lie below these parts remain colorless. In this way, under different UV intensities, different photochromic patterns can be exhibited, which can be quasi-quantitatively distinguished by the naked eye, such as the steering wheel pattern in Figure 1b with each handle having different colors at given UV intensities. The UV photochromic layer and the white background layer are made from mixtures of PDMS with photoswitchable materials and  $\text{TiO}_2$ , respectively, and the latter is used to avoid the interference from the skin color (Figure S8, Supporting Information). Detailed information on the fabrication process can be found in the Experimental Section.

Figure 1c demonstrates the chemical structure of the photoswitchable materials. Three different photoswitchable materials are used in this work, namely, Spiro(2H-indole-2,3'-(3H)naphth(2,1-B)(1,4)oxazine) (SINO), 1,3,3-trimethylindolino-6'-(1-piperidiny)spironaphthoxazine (TPSO), and 3,3-diphenyl-3H-naphtho[2,1-b]pyran (DNP). SINO and TPSO belong to the spirobenzoyran derivatives and spirobenzoyrans are a widely studied chemical class of compounds that exhibit photochromism.<sup>[27]</sup> They consist structurally of a pyran ring, usually a 2H-1benzopyran, linked via a common spiro group to another heterocyclic ring. With higher energy irradiation of UV light (UV range of the 200 to 400 nm) the colorless spirobenzopyran causes heterolytic cleavage of the carbon–oxygen bond, forming the colored merocyanine ring-opened isomers (blue color for SINO and magenta color for TPSO in this work). It should be noted that these photoexcited isomers can be reversed to their original colorless structures by shining lower energy light, usually in the visible range (400–700 nm). The DNP belongs to the chromenes derivative, whose mechanism is similar to that of spirobenzoyrans. Under the influence of UV, the C–O bond in the pyran ring is broken to offer a trans-quinoidal form, which exhibits a colored state (yellow color for DNP); under the illumination of visible light, the colored state recovers to its colorless photostationary state. By combining the three-elemental colors (blue, magenta, and yellow), more color variety of photochromic materials can be obtained, for example, green (blue + yellow) and brown (blue + magenta), thus capable of extending its aesthetic applications and demonstrating its advantages over single-color UV sensors.<sup>[28–30]</sup> We tested the

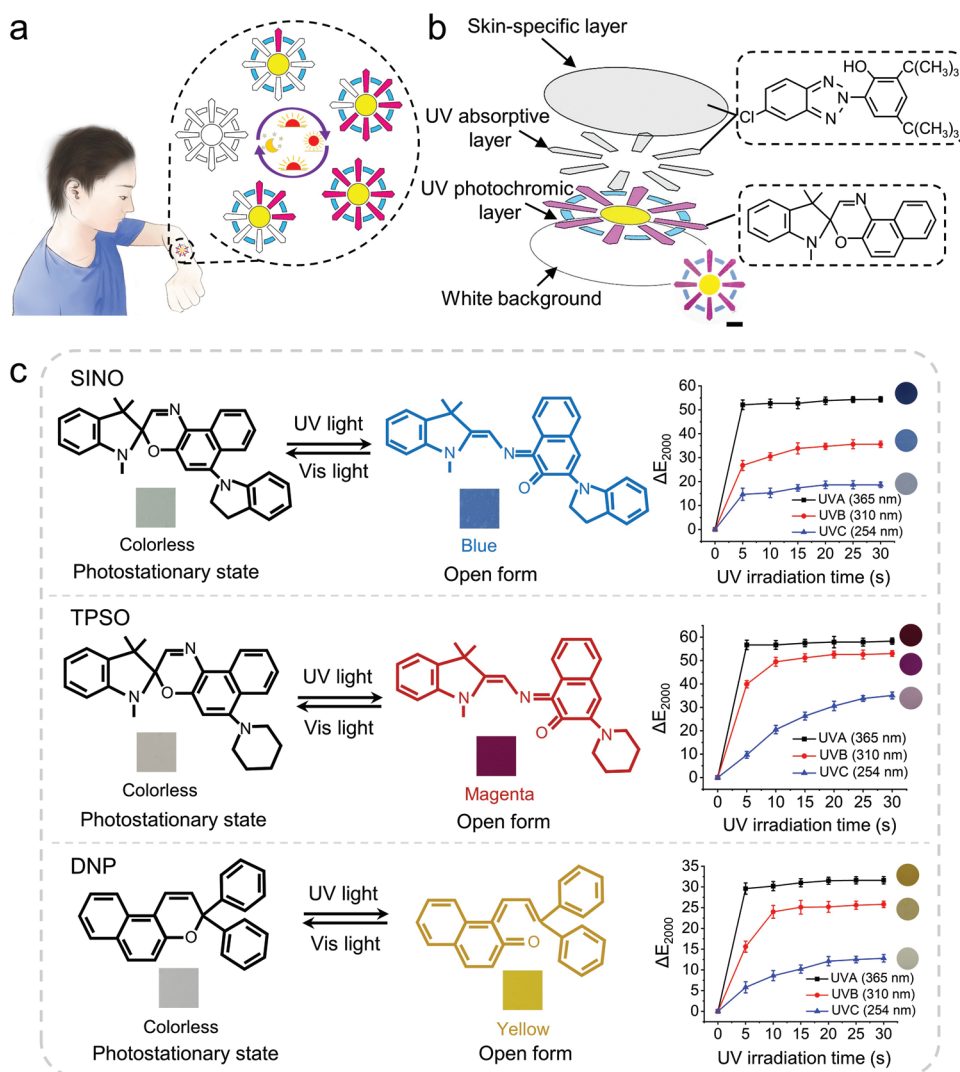


**Figure 1.** Schematic diagram of the ultraviolet (UV) sensor. a) Epidermal UV sensor showing different color patterns following the changing of UV intensity. b) Components of the UV sensor. The insert shows a picture of the UV sensor. c) The chemical structure and UV selective performance of photoswitchable materials.  $n = 3$  independent experiments were conducted with the data shown as  $\pm$  s.d. Scale bar is 1cm.

color changing performance of the three photoswitchable materials by applying different regions of the UV spectrum: UVA (365 nm, SV47-UCL, Alonefire, China), UVB (310 nm, UV310, Starshine, China), and UVC (254 nm, Starshine, China) with the same intensity of  $20 \text{ W m}^{-2}$ . To reflect the color differences perceived by the human eye, CIEDE2000 ( $\Delta E_{2000}$ ) color difference formulas were applied to characterize the color changing performance.<sup>[31]</sup> It can be seen that the three materials respond differently to UVA, UVB, and UVC, where the  $\Delta E_{2000}$  value decreases following the application of UVA, UVB, and UVC, respectively. For the SINO material, after 30 s UV irradiation, the  $\Delta E_{2000}$  value for UVC is 18.7 and for UVA and UVB, it is 54.4 and 35.6, respectively, which provide observable color differences. Meanwhile, the photoswitchable materials demonstrate different color changing rate for UVA, UVB, and UVC, offering UVR spectral selectivity. The UVC saturates the sensor in about 20 s and as a comparison, the saturating time for UVA and UVB is about 5 and 10 s, respectively. Although the three

materials have UV selective potentials, following the recommendation of World Health Organization (WHO; Table 1), the UV index containing the whole UV spectrum is applied for the following study.

## 2.2. Characterization of the UV Photochromic and Absorptive Materials

Figure 2a shows a characterization of photochromic materials. Different photochromic layers were put under the illumination of a UV bulb and sunlight, separately. The UV intensity from the UV bulb (2K150, Xingchuang Electronics Co., Ltd) and the sunlight were measured through a commercially available UV meter (LH-125, Lianhuicheng Technologies Co., Ltd). The images were captured using a digital camera (Huawei mate 20) and analyzed using the software Photoshop CS6. More information can be found in the Experimental Section. It can be seen

**Table 1.** Ultraviolet (UV) intensity levels and World Health Organization (WHO) recommended protections.

UV intensity [ $\text{W m}^{-2}$ ]	UV index	MED <sup>a)</sup> time [min]	Recommended protections
<5	0–2	100–180	No protection required.
5–10	3,4	60–100	Protection required: Seek shade during midday hours. Slip on a shirt, slop on sunscreen, and slap on a hat.
10–15	5,6	30–60	
15–30	7–9	20–40	
$\geq 30$	$\geq 10$	<20	Extra protection: Avoid being outside during midday hours. Make sure to seek shade. Shirt, sunscreen, and hat are a must.

<sup>a)</sup>The MED (minimal erythral dose) time is the time people may have erythral response under certain ultraviolet (UV) intensity.

from Figure 2a that for the red color under bulb light, when the UV intensity is  $12.5 \text{ W m}^{-2}$ , the  $\Delta E_{2000}$  is 53.6; and as the UV intensity decreases to  $0.1 \text{ W m}^{-2}$ , the  $\Delta E_{2000}$  can still be 22.9, which can be distinguished by the naked eye. Moreover, up to 30 cycles of color change and recovery can be achieved without compromising the color difference performance (Figure 2bi and Movie S1, Supporting Information), which enables repeated and continuous monitoring of UV intensity. From one color change and recovery cycle (Figure 2bii, Figure S6, Supporting Information), it takes about 7 s for the photochromic material to change from colorless to a saturated color state, and it takes about 15 s for it to recover to its original colorless state, making the whole color change and recovery cycle less than 30 s.

Although the photoswitchable materials used in this paper demonstrate advantages of high sensitivity and continuous monitoring potential, their color change range is still limited, meaning color differences are indistinguishable when the UV intensity is more than  $7 \text{ W m}^{-2}$  (Figure 2c), corresponding to UV index range of 3 (Table 1). To solve this issue, a UV absorptive layer is applied on the surface layer of the photochromic layer to tune the UV intensity reaching this layer. Several absorptive materials were characterized and Figure 2d shows the transmittance-wavelength curve for different absorptive materials, namely 2-(2'-hydroxy-3',5'-di-tert-butylphenyl)-5-chlorobenzotriazole (HD-CB), 2-(2'-hydroxy-3',5'-dipentylphenyl)benzotriazole (HDP), octrizole (OTZ), octabenzone (OTB), and 1H-benzotriazole (HBT) using a pure PDMS layer as a control group. It should be noted that the concentration of all the absorptive materials here is 9%. It can be found that the transmittance for all the UV absorptive materials decreased to almost 0% in the UV region, showing highly effective UV blocking capabilities. Among the UV absorptive materials, HD-CB has the highest transmittance of about 82% in the visible light region, which is comparable to that of the pure PDMS control group (transmittance of 90%). Encouraged by its high transmittance in the visible light region, its transmittance in the UV region was studied for different HD-CB concentrations, ranging from 5.7% to 10% (Figure 2e). As shown in Figure 2e, the transmittance in the UV region exhibits an increasing gradient with increasing HD-CB concentration, and that in the visible light region with different HD-CB concentrations is all above 75%. In fact, the absorptive material concentration (5%–10%) and the mean absorbance in the UV spectrum demonstrate a linear relationship with a calibration curve of  $y = 5.069x + 47.939$  and  $R^2 = 0.987$  (Figure S7, Supporting Information) with  $y$  as the absorbance and  $x$  as the material concentration. Thus, by applying the HD-CB layer

with different concentration on the surface of the photochromic layer, the color changing range is potentially extended. It can be seen in Figure 2c that the detectable UV intensity is extended to  $20 \text{ W m}^{-2}$  by applying the absorptive layer with a concentration of 9%, and meanwhile the minimum detection limit is about  $1.6 \text{ W m}^{-2}$ , meaning an equivalent UV index of 7–9 (Table 1) can be differentiated through naked eye.

### 2.3. UV Sensor Pattern Varieties

The influence of solar UV exposure on human skin is usually evaluated via an erythral response function,<sup>[32]</sup> which is a UV radiation-induced inflammatory response that appears as a reddening of the human skin and is related to both the radiation intensity ( $\text{W m}^{-2}$ ) and the exposure time (s). A minimum erythral dose (MED, in the unit of  $\text{J m}^{-2} = \text{W m}^{-2} \text{ s}$ ) is thus considered a threshold dose for UV radiation, beyond which a particular skin type will produce an erythral response. WHO provides guidance for UV intensity and protection from erythema<sup>[33]</sup> (Table 1). When UV intensity is below  $5 \text{ W m}^{-2}$  (corresponding UV index of 0–2), humans can stay in the sunlight for 100–180 min with no worry for an erythral response. However, when the UV intensity increases to  $15\text{--}30 \text{ W m}^{-2}$  (corresponding a UV index of 7–9), an erythral response may appear in just 20 min, and the WHO recommends seeking shade during midday hours, wearing appropriate clothing, applying sunscreen, and using a hat. According to WHO guidance (Table 1) and the combination strategy of the photochromic and absorptive materials, several UV sensor patterns have been designed (Figure 3), including a steering wheel (pattern A), a flower (pattern B), a Christmas tree (pattern C), and an umbrella (pattern D). To achieve quasi-quantitative naked-eye monitoring capabilities, the following combination strategy for photochromic and absorptive materials is adopted: the sensing areas of all the UV patterns are divided into four parts, indicating a UV index 3, 5, 7, and 9. The concentration of photochromic material for all the sensing areas is 15%, which is measured as having the maximum color difference under UV exposure (Figure S5, Supporting Information). The concentrations of absorptive materials for the four sensing areas are 0%, 3%, 5%, and 9%, respectively, leading to a UV-dependent colorimetric performance based on the characterization results of the materials. For example, when the UV index of 3 is applied, only one handle in pattern A turns red, and as the UV index increases from 3 to 9, the number of colored handles increases

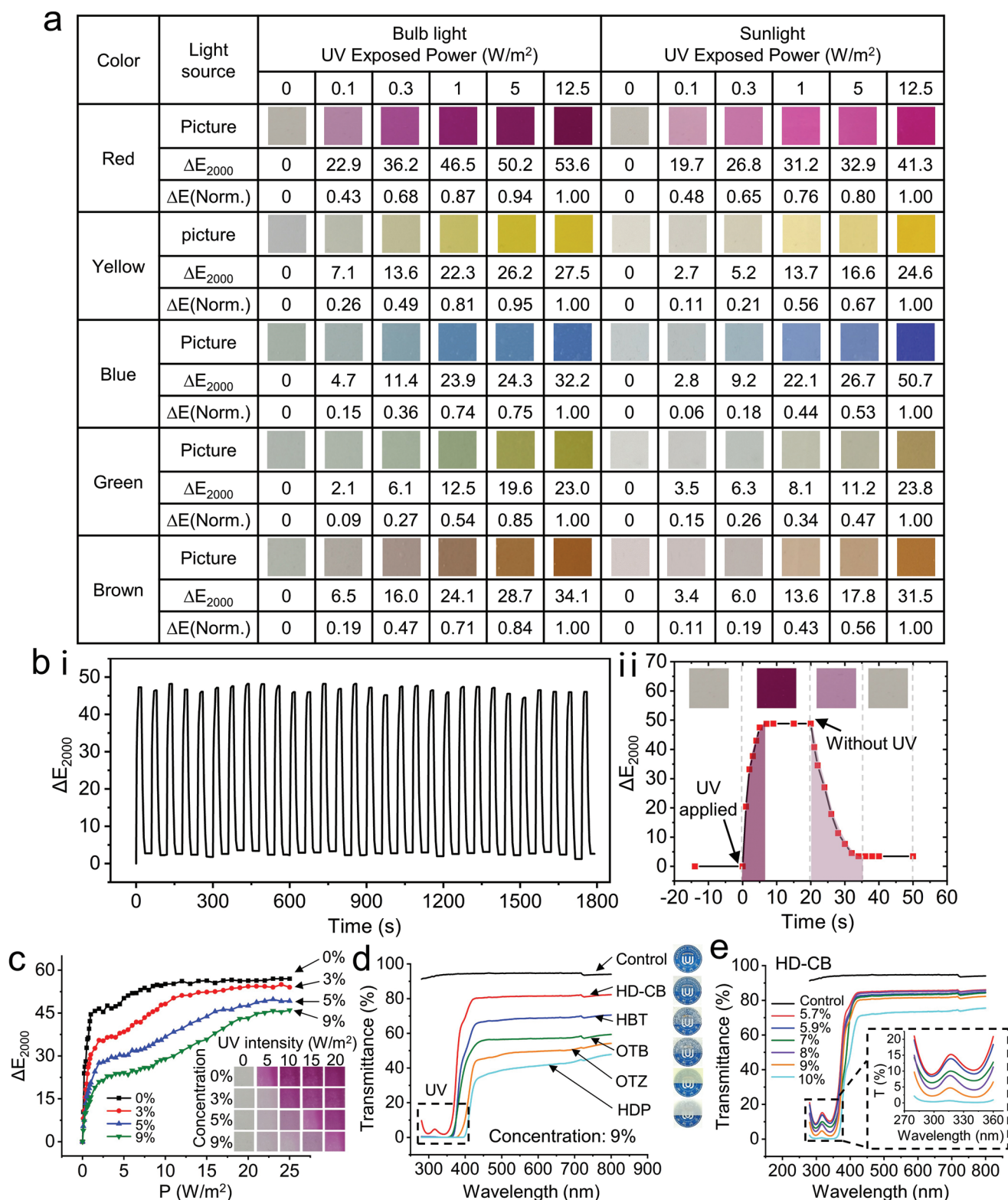


**Figure 2.** Characterization of ultraviolet (UV) photochromic and absorptive materials. a) Color changing images for various photochromic materials with different UV intensity. b) i) Curve of the color change and recovery cycles. ii) One cycle of the color change and recovery with the representative images. c) Curve showing the relationship between color difference and UV intensity with UV absorptive layers of different concentrations. The insert demonstrates the representative images. d) Relationship between transmittance and wavelength from 200 to 800 nm using different UV absorptive materials. The insert pictures show the Westlake University logo covered by the films containing different UV absorptive materials. e) Relationship between transmittance and wavelength from 200 to 800 nm using HD-CB material. The insert shows the transmittance from 280 to 360 nm.

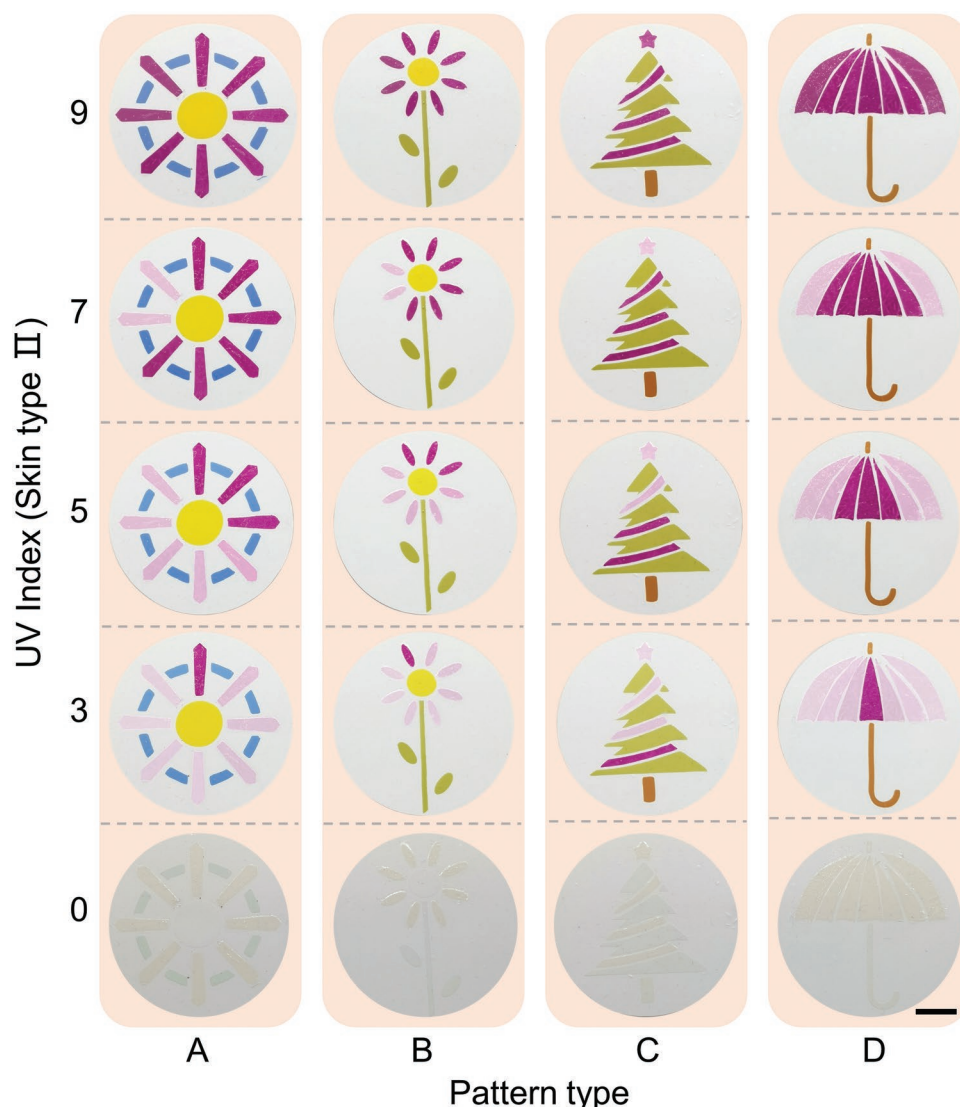


**Figure 3.** Images for different ultraviolet (UV) sensor patterns under different UV index. Scale bar is 1 cm.

from 1 to 3, 5, and 8. When all the eight handles in pattern A are lighted, it indicates that the current UV index is above 9 (UV intensity of about  $30 \text{ W m}^{-2}$ ), and special protection like sunscreen application must be adopted immediately based on WHO guidance.

#### 2.4. Skin-Color Specific Capabilities

As stated in the introduction section, people with different skin types need different UV doses to function well. Specifically, a UV dose of  $200 \text{ J m}^{-2}$  may cause an erythema response to skin type I,<sup>[23]</sup> but may not reach the requirement for people with skin type VI to produce enough Vitamin D. It should be also noted that the UV sensor patterns in Figure 3 are all designed for primarily the skin type II population. To address the skin-color specific issue, six custom-designed UV sensors were developed for people with different skin types based on the corresponding MED thresholds,<sup>[23]</sup> which is achieved by applying

the skin-specific layers with different concentrations of absorptive materials on the surface of the sensor. It can be seen from Figure 4 that six concentrations of absorptive materials are optimized for applying on the sensor surface, ranging from 0.5% to 5.0%. By applying the skin-specific layer with 0.5% absorptive material, the first bar of the UV sensor starts to change color under the UV dose  $50 \text{ J m}^{-2}$  for people with skin type I, while for the other five skin types, the UV sensors remain colorless due to the absorptive layer with higher concentrations, which is still capable of blocking the UV exposure. As the UV dose increases to  $300 \text{ J m}^{-2}$ , all the sensing bars are lighted for skin type I, which indicates the need for immediate sunscreen application or other necessary protections. For skin type VI, only the first bar is lighted which indicates it is safe for these people to stay in the sunlight for a long time. It is notable that each of the sensors covered here with different skin-specific layers retain their individual ability to provide UV index, ranging from 3 to 9. Moreover, to achieve skin-color specificity, only the absorptive material concentration is adjusted for the skin-specific layer

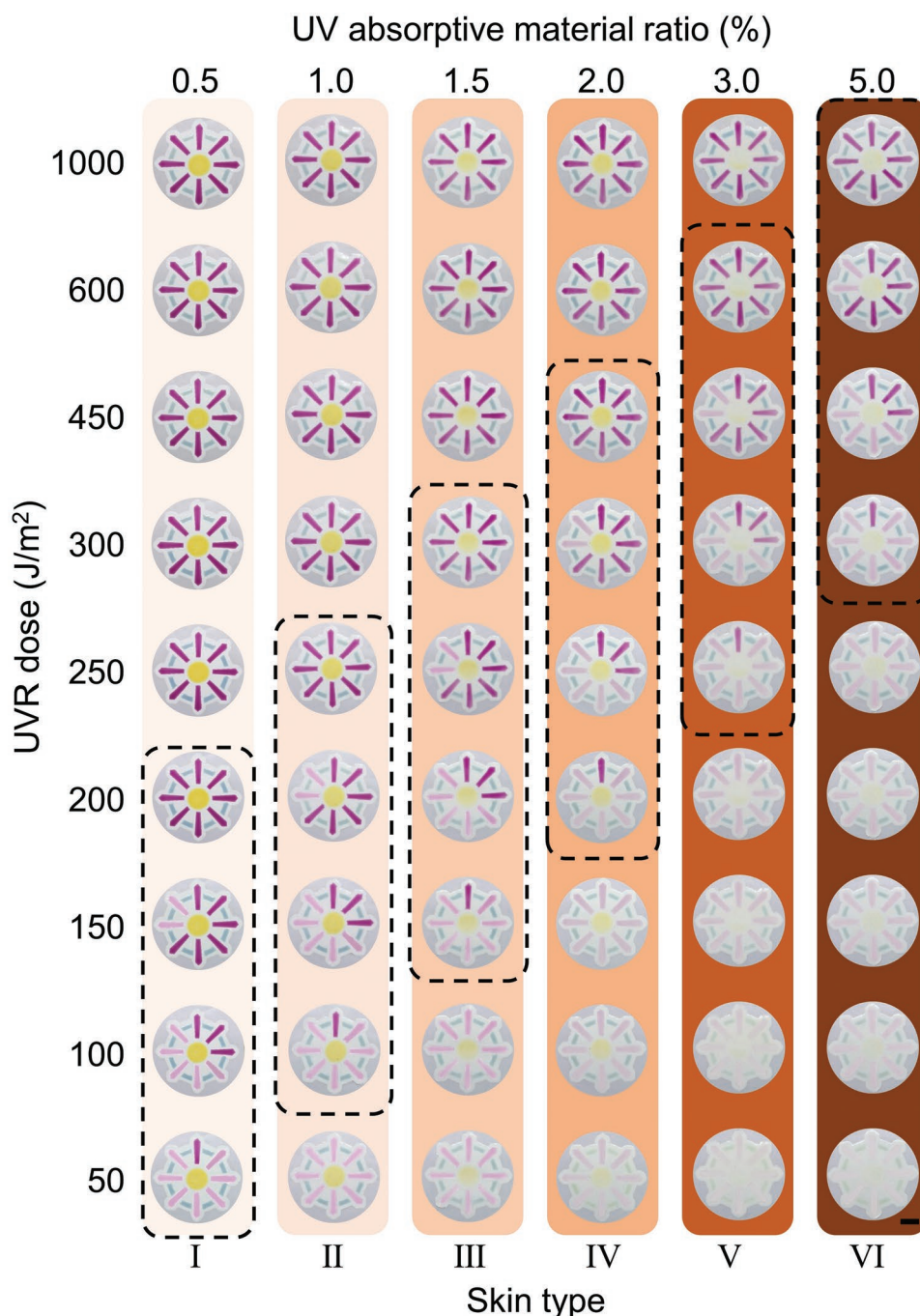


**Figure 4.** Images for the skin-specific performance. Skin specificity is achieved by an appropriate combination of the ultraviolet (UV) sensor covered by skin-specific filter containing different concentration of UV absorptive materials (0.5%–5.0%). Scale bar is 1 cm.

with its thickness remaining 25  $\mu\text{m}$ , demonstrating the advantages of high skin conformability and transmittance over the multilayer optical filter method.<sup>[25]</sup>

## 2.5. UV Sensor Application

Figure 5a shows the stress–strain curves for materials used in each layer measured by dynamic mechanical analysis

(JHY-5KN, Xingsuo Intelligent Instruments Co., Ltd) in tensile mode. Young's modulus of PDMS, photochromic layer, absorptive layer, and  $\text{TiO}_2$  layer is 1.9, 0.2, 0.6, and 2.6 MPa, respectively. The combination of these layers makes the whole UV sensor soft and compatible to human skin (the Young's modulus of normal human skin is 0.42–0.75 MPa.<sup>[34]</sup>), which can be readily compressed, pinched, or stretched (Movie S2, Supporting Information) after applying to the skin using medical adhesives (EX-552, Dup Co. JP). We tested the biocompatible

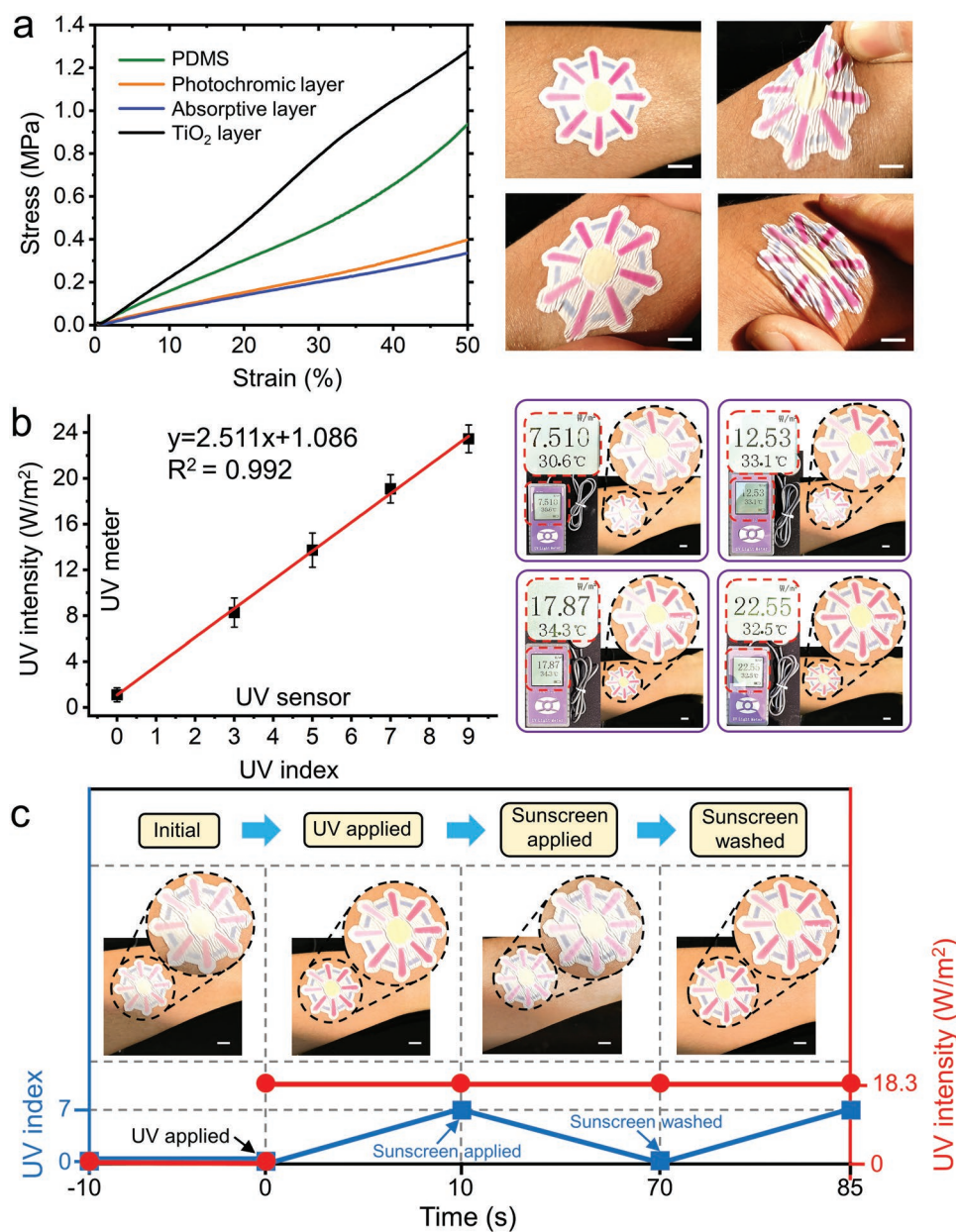


**Figure 5.** Images for the ultraviolet (UV) sensor functionality. a) Stress–strain curves for materials used in each layer. The images demonstrating skin conformability. b) Evaluation of relationship between UV sensor in this work and commercially available UV meter with the representative images.  $n = 3$  independent experiments were conducted with the data shown as  $\pm$  s.d. c) Detection results after applying and washing sunscreen with the UV intensity of  $18.3 \text{ W m}^{-2}$ . Scale bar is 1 cm.

performance of the epidermal UV sensors. The volunteer reads, walks, and does sports as usual wearing the epidermal UV sensor for 1 day (Figure S9a, Supporting Information). According to the volunteer, it can hardly feel the existence of the UV sensor when wearing it and after removing the sensor, there are no allergy reactions or other bad effect to the skin (Figure S9b, Supporting Information). Figure 5b compares the UV index obtained from the present UV sensor and the UV intensity measured from a commercially available UV meter, where a linear relationship was shown with a calibration curve of  $y = 2.511x + 1.086$  and  $R^2 = 0.992$ . Photos in

Figure 5b clearly show the process of color changing when the measured UV intensity varies from  $75 \text{ W m}^{-2}$  (or equivalently UV index of 3) to  $22.5 \text{ W m}^{-2}$  (or equivalently UV index of 9). Due to the skin conformability of the UV sensor, sunscreen can be directly applied to the sensor surface, providing an executive way to protect the skin with the help of the present UV sensor. It can be seen from Figure 5c that when no UVR is applied, the UV sensor shows no colored patterns. As the UV intensity of  $18.3 \text{ W m}^{-2}$  is applied, six handles of the UV sensor are lighted, indicating a UV index of 7, which is in agreement with the guidance from the WHO. When the sunscreen is applied,



the color of the sensing handles fades to a colorless state in about 60 s. Furthermore, after washing the sunscreen using DI water, the six sensing handles change colors again in about 15 s, which indicates the UV sensor operates with repeated and continuous UV monitoring potential. It is notable that the color change/recovery time for the sunscreen application (about 75 s) is longer than that of the UV-bulb experiments (about 30 s, Figure 2bii). This is because the sunscreen cannot block the UV energy immediately and it takes a period of time for the sunscreen to generate a UV protective layer.

### 3. Conclusion

In this paper, we presented a material and design strategy for epidermal UV sensors with the following features: (1) naked-eye quasi-quantitative monitoring capabilities (UV index ranging from 3 to 9 can be distinguished by the naked eyes with comparable results to a commercially available UV meter), (2) long-term durability (UV sensing performance remains almost unchanged after 30 cycles of UV exposures), (3) real-time monitoring capability (the sensing color can change and recover in less than 30 s), (4) skin conformability (the UV sensor is soft and can be applied directly on the skin), and (5) skin-color specificity (the UV sensor can be customized for people with different skin types). We compare our UV sensor with the state-of-art UV sensing technologies (Table S1, Supporting Information) and to the best of our knowledge there are no UV sensors that simultaneously possess all these features. The UV sensors demonstrated here, however, are of limited functionality: they lack the capability of monitoring cumulative UV doses, which means as long as the UV intensity remains the same, the sensing color does not change with increase in exposure time. However, most of the UV sensor with the cumulative UV dose monitoring capability can only be applied once, since the cumulative color cannot recover to the original state. Real-time UV intensity monitoring is critical to enable people to take protections before UV radiation causes damages to the skin. In our daily life, it is more desirable for UV sensors to have the capability of real-time and continuous monitoring of the UV intensity or UV index as a whole, which is a measure that the WHO uses to guide people on UV protection.

### 4. Experimental Section

**Study Participant:** The human participant study was approved by the Ethics Commission of Westlake University in Hangzhou (20220725)HQ001). Informed consent was obtained from all the participants.

**Materials:** The PDMS (SYLGARD 184 Silicone Elastomer Kit) was purchased from Dow Chemical Co. The photochromic materials (Spiro(2H-indole-2,3'-(3H)naphth(2,1-B)(1,4)oxazine), 1,3,3-trimethylindolino-6'-(1-piperidinyl)spironaphthoxazine, and 3,3-diphenyl-3H-naphtho[2,1-b]pyran) were purchased from Insilico Co., Ltd. The UV absorptive materials 2-(2'-hydroxy-3',5'-di-tert-butylphenyl)-5-chlorobenzotriazole, 2-(2'-hydroxy-3',5'-dipentylphenyl)benzotriazole, octrizole, octabenzone, and 1H-benzotriazole were purchased from Dinghai Plastic Chemical Co., Ltd. TiO<sub>2</sub> (R-258) was purchased from Pangang Group Titanium Industry Co., Ltd. Medical adhesives (EX-552) and sunscreen spray (SPF50+) were purchased from Duo Co., JP and RECIPE Co., Ltd., respectively.

**Fabrication Process:** The UV photochromic powder was mixed with a PDMS precursor (part A: part B = 10:1) at a weight ratio of 15%. Different amounts of UV absorptive powders were mixed with PDMS precursors (part A: part B = 10:1) separately, at a weight ratio of 3%, 5% and 9% for the absorptive layer and at a weight ratio of 0.5%, 1.0%, 1.5%, 2.0%, 3.0%, and 5.0% for the skin-specific layer. TiO<sub>2</sub> powders were mixed with PDMS precursors (part A: part B = 50:3) at a ratio of 40%. The pictures of the above-mentioned material powders and mixed pastes can be found in Figure S1 (Supporting Information). Figure S2 (Supporting Information) demonstrates the schematic diagram of the fabrication process. First, the mask 1 was applied on a PMMA substrate and the TiO<sub>2</sub> paste was coated on mask 1 and heated for 5 min at 110 °C on a hot plate. Then, mask 2 was applied on the patterned TiO<sub>2</sub> layer, coated with photochromic pastes and heated for 3 min at 95 °C. Next, mask 3 was applied on the patterned photochromic layer, coated with absorptive pastes at a weight ratio of 3%, 5%, and 9%, and heated for 3 min at 95 °C. Next, mask 1 was applied on the patterned absorptive layer, coated with absorptive pastes at a weight ratio of 0.5%, 1.0%, 1.5%, 2.0%, 3.0%, and 5.0% for different skin types, and heated for 3 min at 95 °C. Finally, the UV sensors were peeled off from the PMMA substrate. All the masks used in the fabrication process can be found in Figure S3 (Supporting Information). It should be noted that the UV sensor can be mass fabricated by using the screen printing and lamination method (Figure S4, Supporting Information).

**Strain–Stress Test:** Samples of PDMS, photochromic layer, absorptive layer, and TiO<sub>2</sub> layer were prepared for measurement in tensile mode by dynamic mechanical analysis (JHY-5KN, Xingsuo Intelligent Instruments Co., Ltd). The dimension of the samples was 10 × 5 × 0.025 mm with a strain rate of 10% min<sup>-1</sup> up to 50%.

**UV Exposure and UV–Vis Test:** The UV exposure was performed under UV bulbs (2K150-2000W, Xingchuang Electronics Co., Ltd) and sunlight. The UV intensity was measured using a commercially available UV meter (LH-125, Lianhuicheng Technologies Co., Ltd). Transmittance and absorbance of UV photochromic and absorptive materials were measured using a spectrophotometer (UV-3600i Plus, Shimadzu) in the spectra range of 200–800 nm. The testing samples were the same as those used in the experiments.

**Color Difference Calculation Method:** The images of the testing samples were captured with a digital camera (Huawei mate 20, Huawei Technologies Co., Ltd) after the samples were put under a UV bulb and sunlight. The images were analyzed using Photoshop CS6 to extract a single averaged sRGB values. The color difference was calculated using CIE 2000 Color-Difference Formula.<sup>[31]</sup>

**Statistical Analysis:** All testing results are presented as means ± s.d. after repeating at least three times using separate UV sensors unless otherwise specified. No data were excluded from the analyses.

### Supporting Information

Supporting Information is available from the Wiley Online Library or from the author.

### Acknowledgements

Some of the experimental work was conducted using the facilities at Arizona State University when C.L. and H.J. were at that institution. H.J. acknowledges support from Westlake University.

### Conflict of Interest

The authors declare no conflict of interest.

## Data Availability Statement

The data that support the findings of this study are available from the corresponding author upon reasonable request.

## Keywords

epidermal, naked-eye quasi-quantitative, skin-color specific, UV sensor

Received: September 8, 2022

Revised: October 27, 2022

Published online:

- [1] Y. Matsumura, H. N. Ananthaswamy, *Toxicol. Appl. Pharmacol.* **2004**, 195, 298.
- [2] D. F. Macfarlane, C. A. Alonso, *Arch. Dermatol.* **2009**, 145, 447.
- [3] Australian Institute of Health and Welfare, *GRIM (General Record of Incidence of Mortality) Books*, AIHW, Canberra **2013**.
- [4] M. P. Staples, M. Elwood, R. C. Burton, J. L. Williams, R. Marks, G. G. Giles, *Med. J. Aust.* **2006**, 184, 6.
- [5] L. G. Gordon, D. Rowell, *Eur. J. Cancer Prev.* **2015**, 24, 141.
- [6] A. R. Webb, L. Kline, M. F. Holick, *J. Clin. Endocrinol. Metab.* **1988**, 67, 373.
- [7] M. Gröbner, J. Gröbner, G. Hülsen, *Photochem. Photobiol. Sci.* **2015**, 14, 352.
- [8] M. K. B. Bogh, A. V. Schmedes, P. A. Philipsen, E. Thieden, H. C. Wulf, *J. Invest. Dermatol.* **2010**, 130, 546.
- [9] M. Begum, A. Hocking, D. Miskelly, *Int. J. Food Microbiol.* **2009**, 129, 74.
- [10] H. Inagaki, A. Saito, H. Sugiyama, T. Okabayashi, S. Fujimoto, *Emerging Microbes Infect.* **2020**, 9, 1744.
- [11] P. Wang, Y. Wang, L. Ye, M. Wu, R. Xie, X. Wang, X. Chen, Z. Fan, J. Wang, W. Hu, *Small* **2018**, 14, 1800492.
- [12] G. Dubourg, M. Radović, *ACS Appl. Mater. Interfaces* **2019**, 11, 6257.
- [13] Z. Zhang, Y. i Ning, X. Fang, *J. Mater. Chem. C* **2019**, 7, 223.
- [14] L. Li, Z. Liu, L. Wang, B. Zhang, Y. Liu, J. - P. Ao, *Mater. Sci. Semi-cond. Process.* **2018**, 76, 61.
- [15] P. Zhou, C. Chen, X. Wang, B. Hu, H. San, *Sens. Actuators, A* **2018**, 271, 389.
- [16] S. Pyo, J. Choi, J. Kim, *Adv. Electron. Mater.* **2019**, 5, 1800737.
- [17] A. V. Parisi, M. G. Kimlin, *Photochem. Photobiol.* **2004**, 79, 411.
- [18] P. W. Schouten, A. V. Parisi, D. J. Turnbull, *Photochem. Photobiol.* **2010**, 86, 706.
- [19] J. Wang, A. S. Jeevarathinam, A. Jhunjunwala, H. Ren, J. Lemaster, Y. Luo, D. P. Fenning, E. E. Fullerton, J. V. Jokerst, *Adv. Mater. Technol.* **2018**, 3, 1800037.
- [20] H. Araki, J. Kim, S. Zhang, A. Banks, K. E. Crawford, X. Sheng, P. Gutruf, Y. Shi, R. M. Pielak, J. A. Rogers, *Adv. Funct. Mater.* **2017**, 27, 1604465.
- [21] E. Dumont, S. Banerjee, M. Contreras, *US 2016/0364131A1* **2016**.
- [22] Y. Shi, M. Manco, D. Moyal, G. Huppert, H. Araki, A. Banks, H. Joshi, R. McKenzie, A. Seewald, G. Griffin, E. Sen-Gupta, D. Wright, P. Bastien, F. Valceschini, S. Seité, J. A. Wright, R. Ghaffari, J. Rogers, G. Balooch, R. M. Pielak, *PLoS One* **2018**, 13, 0190233.
- [23] T. B. Fitzpatrick, *Arch. Dermatol.* **1988**, 124, 869.
- [24] W. Zou, M. Sastry, J. J. Gooding, R. Ramanathan, V. Bansal, *Adv. Mater. Technol.* **2020**, 5, 1901036.
- [25] W. Zou, A. González, D. Jampaiah, R. Ramanathan, M. Taha, S. Walia, S. Sriram, M. Bhaskaran, J. M. Dominguez-Vera, V. Bansal, *Nat. Commun.* **2018**, 9, 3743.
- [26] P. S. Khiabani, A. H. Soeriyadi, P. J. Reece, J. J. Gooding, *ACS Sens.* **2016**, 1, 775.
- [27] P. Bamfield, M. Hutchings, *Chromic Phenomena: Technological Applications of Colour Chemistry*, 3rd ed., The Royal Society of Chemistry, London **2018**, p.11.
- [28] S. Cai, C. Zuo, J. Zhang, H. Liu, X. Fang, *Adv. Funct. Mater.* **2021**, 31, 2100026.
- [29] J. Kim, G. A. Salvatore, H. Araki, A. M. Chiarelli, Z. Xie, A. Banks, X. Sheng, Y. Liu, J. W. Lee, K.-I. Jang, S. Y. Heo, K. Cho, H. Luo, B. Zimmerman, J. Kim, L. Yan, X. Feng, S. Xu, M. Fabiani, G. Gratton, Y. Huang, U. Paik, J. A. Rogers, *Sci. Adv.* **2016**, 2, e1600418.
- [30] E. Hacker, C. Horsham, H. Ford, G. Hartel, C. M. Olsen, N. Pandeya, M. Janda, *Prev. Med.* **2019**, 124, 67.
- [31] M. R. Luo, G. Cui, B. Rigg, *Color Res. Appl.* **2001**, 26, 340.
- [32] R. Lucas, T. McMichael, W. Smith, B. Armstrong, in *Solar Ultraviolet Radiation: Global Burden of Disease from Solar Ultraviolet Radiation* (Eds: A. Prüss-üstün, H. Zeeb, C. Mathers, M. H. Repacholi), World Health Organization, Geneva **2006**, p. 250.
- [33] World Health Organization, World Meteorological Organization, United Nations Environment Programme, *International Commission on Non-Ionizing Radiation Protection, Global Solar UV Index: A Practical Guide*, **2002**, p. 8.
- [34] J. A. Clark, J. C. Y. Cheng, K. S. Leung, *Burns* **1996**, 22, 443.